www.elsevier.com/locate/jbiomech

Disturbed flow in a patient-specific arteriovenous fistula for haemodialysis: multidirectional and reciprocating near-wall flow patterns

Bogdan Ene-Iordache, Cristina Semperboni, Gabriele Dubini, Andrea Remuzzi

PII: S0021-9290(15)00229-8
DOI: http://dx.doi.org/10.1016/j.jbiomech.2015.04.013
Reference: BM7130

To appear in: *Journal of Biomechanics*

Received date: 12 December 2014
Revised date: 27 March 2015
Accepted date: 5 April 2015

Cite this article as: Bogdan Ene-Iordache, Cristina Semperboni, Gabriele Dubini and Andrea Remuzzi, Disturbed flow in a patient-specific arteriovenous fistula for haemodialysis: multidirectional and reciprocating near-wall flow patterns, *Journal of Biomechanics,* http://dx.doi.org/10.1016/j.jbiomech.2015.04.013

BM-D-14-01223.R1

Disturbed flow in a patient-specific arteriovenous fistula for haemodialysis: multidirectional and reciprocating near-wall flow patterns

Bogdan Ene-Iordache[a], Cristina Semperboni[b], Gabriele Dubini[c] and Andrea Remuzzi[a,d]

[a] IRCCS – Istituto di Ricerche Farmacologiche "Mario Negri"
Ranica (BG), Italy

[b] Department of Biomedical Engineering
Politecnico di Milano
Milano (MI), Italy

[c] Laboratory of Biological Structure Mechanics - LaBS
Department of Chemistry, Materials and Chemical Engineering "Giulio Natta"
Politecnico di Milano
Milano (MI), Italy

[d] Department of Industrial Engineering
University of Bergamo
Dalmine (BG), Italy

Running head: **Disturbed flow in a patient-specific AVF**

Short Communication

Word count = 1,980

Send correspondence to:

Bogdan Ene-Iordache, EngD

Laboratory of Biomedical Technologies

Clinical Research Center for Rare Diseases *Aldo e Cele Daccò*

Via G.B. Camozzi 3, 24020 Ranica (BG), Italy

Tel.: 0039 035 4535390

Fax: 0039 035 4535371

E-mail: bogdan.ene-iordache@marionegri.it

ABSTRACT

Actual surgical creation of vascular access has unacceptable failure rates of which stenosis formation is a major cause. We have shown previously in idealized models of *side-to-end* arteriovenous fistula that disturbed flow, a near-wall haemodynamic condition characterized by low and oscillating fluid shear stress, develops in focal points that correspond closely to the sites of future stenosis. Our present study was aimed at investigating whether disturbed flow occurs in patient-specific fistulae, too.

We performed an image-based computational fluid dynamics study within a realistic model of wrist *side-to-end* anastomosis fistula at six weeks post-surgery, with subject-specific blood rheology and boundary conditions. We then categorized disturbed flow by means of established haemodynamic wall parameters.

The numerical analysis revealed laminar flow within the arterial limbs and a complex flow field in the swing segment, featuring turbulent eddies leading to high frequency oscillation of the wall shear stress vectors. Multidirectional disturbed flow developed on the anastomosis floor and on the whole swing segment. Reciprocating disturbed flow zones were found on the distal artery near the floor and on the inner wall of the swing segment.

We have found that both multidirectional and reciprocating disturbed flow develops on the inner side of the swing segment in a patient-specific *side-to-end* fistula used for vascular access after six weeks post-operatively. This has obvious implications for elucidating the haemodynamic forces involved in the initiation of venous wall thickening in vascular access.

Keywords: Arteriovenous fistula, Neointima formation, Computational fluid dynamics, Multidirectional flow, Reciprocating flow

INTRODUCTION

A well-functioning vascular access (VA) serves as lifeline for the patients on haemodialysis. There is general consensus in the literature on the superiority of autogenous arteriovenous fistulae (AVF) over arteriovenous grafts (AVG) and central venous catheters regarding VA survival, related complications and costs (Leermakers et al., 2013; Vassalotti et al., 2012). Despite the existence of clinical guidelines (NKF/KDOQI, 2006) recommending well-defined criteria to create AVF, a high failure rate has been reported due to formation of juxta-anastomotic stenoses. In studies performed between 1977 and 2002 where VA was provided by AVF (Allon and Robbin, 2002), the mean early failure rate was 25% (range 2% - 53%) while the mean one-year patency rate was 70% (42% - 90%).

Since the '90s computational fluid dynamics (CFD) applied to blood vessels was intensively used to assess the wall shear stress (WSS) in the study of the link between haemodynamics and cardiovascular disease. Beside characterization of the general flow field, many patient-specific CFD studies have focused on the assessment of the so-called "disturbed flow" acting near wall. The pattern of disturbed flow is irregular, it features secondary and recirculation eddies that may change in direction with time and space, and hence it exerts low and oscillating WSS on the endothelial layer (Davies, 2009). Localization of atherosclerosis within specific sites in branch points or curvatures of the arterial tree, in humans and in experimental animals (Chiu and Chien, 2011), led to the concept that the disturbed flow is related to the vascular lesions. Also in VA, recent findings about the localization of these sites matching areas of disturbed flow (Remuzzi and Ene-Iordache, 2013) may add new insights into the mechanism of pathogenesis of neointimal hyperplasia (NH) after the surgical creation of the anastomosis.

By using CFD we have shown that disturbed flow may develop in focal sites of radial-cephalic models of AVF, either in *side-to-end* or *end-to-end* configuration, at least in

idealized geometry with flow conditions resembling the initial days after surgery (Ene-Iordache and Remuzzi, 2012). In that study, we speculated on a local remodelling mechanism for neointima formation induced by the local disturbed flow. The present study was aimed at investigating whether disturbed flow occurs also in a patient-specific AVF model, which would confirm the above hypothesis on the haemodynamics-related mechanism of local development of stenosis.

MATERIALS AND METHODS

Patient-specific data and AVF model

The subject was a 48 year old male, who participated in a prospective clinical trial (Caroli et al., 2013). As per study protocol (Bode et al., 2011), the patient had blood sample, ultrasound (US) and magnetic resonance angiography (MRA) investigations of the left arm vessels, pre-operatively and after six weeks post-operatively. Patient-specific flow rate waveforms derived from US in the arteries, namely the proximal artery (PA) and the distal artery (DA) are shown in Figure 1a. Details on their calculation and about the 3D reconstruction of the AVF model are provided in the Supplemental data on-line.

Since hexahedral meshes are known to reduce the computational costs respect to the tetrahedral ones (De Santis et al., 2011), and to provide higher accuracy in the calculation of WSS (De Santis et al., 2010), we decided to use hexahedral cells for the AVF mesh. The internal volume was discretized with the *foamyHexMesh* mesher which is part of *OpenFOAM* v. 2.3.1 suite (OpenFOAM team, 2014). Starting from the surface geometry, this mesher produced high quality hexahedral grids with regular shape cells. Two thin boundary layers of cells were generated near the wall in order to increase the accuracy of WSS calculation. A coarser mesh with more than 128,000 cells, and two refined, consisting of more than 300,000 and 780,000 cells were generated for the AVF model. After a steady

CFD study for mesh-independence, which yielded a maximum difference in WSS lower than 5% relative to the finest grid, we concluded that the mesh with 300,000 cells resolves accurately the flow field and related WSS inside this type of AVF setting. Full and detailed view of the AVF grid, with highlighted the anastomosis floor and the swing segment (SS) of cephalic vein, are presented in Figure 1b.

CFD simulation of blood flow in the AVF

Transient flow simulation was performed using the *OpenFOAM* code, a multipurpose and well validated CFD tool based on the finite volume method (OpenFOAM team, 2014). We considered blood non-Newtonian (Supplemental data) and assumed density 1.05 g/cm^3.

As boundary conditions we prescribed blood flow rates at the PA and DA inlets with the waveforms shown in Figure 1a, traction-free at the vein outlet and no-slip at the walls. We used *pimpleFoam*, a transient solver for incompressible flows using the PIMPLE (merged PISO-SIMPLE) algorithm and first order Euler time integration scheme. This solver adjusts the time step based on a user-defined maximum Courant–Friedrichs–Lewy (CFL) number, which we set to 1. The numerical simulation ran in 19,940 variable time steps for a cycle, corresponding to a temporal resolution between 0.018 to 0.067 ms, and results were saved for post-processing in 1,000 equal time steps for each cycle. Three complete cardiac cycles were solved in order to damp the initial transients of the fluid and only the results of the third cycle were considered for data processing.

For the PA and DA inlets, and the vein outlet, we calculated the Reynolds and the Womersley numbers as described previously (Ene-Iordache and Remuzzi, 2012). Geometric and haemodynamic features of the patient-specific AVF model are summarized in Table 1.

Data post-processing

We localized reciprocating disturbed flow by means of the oscillatory shear index (OSI) (He and Ku, 1996) and multidirectional disturbed flow by means of the transverse WSS (transWSS) metric (Peiffer et al., 2013). Also, aimed at describing the nature of the haemodynamic shear, we generated plots of WSS magnitude in time in several feature points on the AVF surface. General flow field, WSS patterns, and a video clip showing the evolution of WSS vectors throughout one cardiac cycle were provided as Supplemental material.

RESULTS

The patterns of disturbed flow in this patient-specific AVF are presented in Figure 2. Reciprocating shear disturbed flow zones revealed by high OSI (Figure 2a), are located on the inner wall of the SS, after the vein curvature, and on the DA near the anastomosis floor. Multidirectional flow, as characterized by medium-to-high transWSS (> 10 dyne/cm^2, Figure 2b) is located on the anastomosis floor, the whole SS and, in a lesser extent more distally, after the vein curvature. Such patterns of transWSS indicate that shear vectors change direction throughout the cardiac cycle on the whole SS surface, while they remain approximately parallel to the main direction of flow on the PA and DA walls.

The time-course of the WSS vector throughout the pulse cycle for four feature points on the AVF surface are presented in Figure 3 while their near-wall flow characteristics are summarized in Table 2. These points are shown in Figure 2a and were selected specifically to characterize the shear vector acting on the inner wall of PA (P1) corresponding to laminar bulk flow, matching the highest OSI on the DA and SS (P2 and P3) in disturbed flow zones, and on the outer wall of the vein (P4) after the SS curvature. The graphs reveal high WSS on the PA (P1, time-averaged 78.9 dyne/cm^2), specific for laminar and high blood flow. Pure reciprocating flow develops on the DA, oscillating with the frequency of heart rate and

having a low average (P2, OSI 0.42, time-averaged WSS 0.7 dyne/cm^2). High frequency, either multidirectional or reciprocating flow develops on the inner wall of the SS (P3, transWSS 22.7 dyne/cm^2, OSI 0.47 and time-averaged 2.1 dyne/cm^2). More distally on the outer vein, the WSS pattern is multidirectional lowered (P4, transWSS 6.1 dyne/cm^2) and oscillating with high frequency around a big value (time-averaged 66.7 dyne/cm^2). The evolution of the WSS vectors throughout the cardiac cycle in the featured points above can be well observed in the Supplemental video clip.

DISCUSSION

While the mechanism of vessel wall pathophysiology has been subject of much research, the idea of the link between disturbed flow and NH in VA is relatively new (Remuzzi and Ene-Iordache, 2013). In the present study we employed image-based CFD in a realistic model of *side-to-end* radial-cephalic AVF, showing development of disturbed flow. The working hypothesis regarding existence of disturbed flow zones that may trigger the local remodelling mechanism (Ene-Iordache and Remuzzi, 2012), was corroborated also in this patient-specific AVF case. Our study is in agreement with previous idealized geometry (Ene-Iordache et al., 2013; Niemann et al., 2010) and image-based CFD studies (He et al., 2013) that reported development of reciprocating disturbed flow (high OSI) on the AVF walls.

This is the first study to reveal the multi-directionality of WSS on the anastomosis floor and on the SS walls. The high values of transWSS in Figure 2b are indicative for development of complex vortices that rotate also the shear stress vectors on the vessel wall. At the same time, in some areas of the inner wall of the SS, reciprocating disturbed flow develops as shown in Figure 2a. Another novel finding was to show that the nature of reciprocating flow developed on DA and SS walls are different. While the DA experienced pure reciprocating flow at the

frequency of the heart rate, the oscillations of the WSS on the SS wall were at high frequencies, induced by the turbulent bulk flow at this level.

Our results are confirmed by an *in vivo* study in canines (Jia et al., 2015) showing that NH develops more on the inner compared to the outer wall of SS, and compared with the proximal vein. Also, in a clinical study (Marie et al., 2014), serial AVF patients were showing development of turbulence only in the SS, while spiral laminar flow developed in the PA and distally in the draining vein. By solving the numerical solution with a very high temporal resolution we could catch the transition from laminar to turbulent flow that develops in the SS, in line with similar findings of other authors (Lee et al., 2007; McGah et al., 2013).

Our study has obvious implications for elucidating the haemodynamic forces involved in the initiation of venous wall thickening in VA. The high frequency shear oscillations on the SS wall, having a low time-averaged WSS, may trigger or enhance venous NH. A similar conclusion was achieved by (Himburg and Friedman, 2006), showing that regions of porcine iliac arteries with increased endothelial permeability experience higher frequency oscillations in shear. While there is considerably evidence *in vitro* on laminar pulsatile vs. oscillatory shear, demonstrating clearly the atherogenic effect of pure reciprocating flow on the endothelium (Chiu and Chien, 2011), few data exist in literature on the effect of multidirectional WSS.

Among the limits of the work, the study of only one patient-specific model with no longitudinal data is recognised, recalling the need of further larger studies. We also did not include the compliance of the wall in the AVF model. McGah et al. (McGah et al., 2014) studied the effects of wall distensibility, finding lower time-averaged WSS compared to the rigid-walled simulation in a *side-to-end* AVF, but whether this affects also the near-wall disturbed flow should be further investigated. However, the technologies available today allow to optimize anastomotic geometries (Walsh et al., 2003) or to conduct longitudinal

patient-specific studies for the follow-up of VA adaptation and local remodelling (He et al., 2013; Sigovan et al., 2013).

In conclusion, in the present study we have studied the local patterns of WSS in a patient-specific *side-to-end* anastomosis, an AVF setting with high blood flow developed at six weeks post-operatively. We have found that the swing segment of the vein is a conduit subjected to multidirectional hemodynamic shear stress and simultaneously develops reciprocating disturbed flow in some focal points. This combination may boost the initiation of NH after the surgically creation of the AVF, leading to subsequent failure of VA.

ACKNOWLEDGEMENTS

Part of this study was presented at the 7th World Congress of Biomechanics held in Boston in July 2014. The authors acknowledge their collaborators from the ARCH-Consortium (project FP7-ICT-2007-2, grant 224390) for patient-data gathering.

Conflict of Interest:

All the authors certify that they have NO affiliations with or involvement in any organization or entity with any financial interest (such as honoraria; educational grants; participation in speakers' bureaus; membership, employment, consultancies, stock ownership, or other equity interest; and expert testimony or patent-licensing arrangements), or non-financial interest (such as personal or professional relationships, affiliations, knowledge or beliefs) in the subject matter or materials discussed in this manuscript.

197 **REFERENCES**

198 Allon, M., Robbin, M.L., 2002. Increasing arteriovenous fistulas in hemodialysis patients:
199 problems and solutions. Kidney Int 62, 1109-1124.

200 Bode, A., Caroli, A., Huberts, W., Planken, N., Antiga, L., Bosboom, M., Remuzzi, A.,
201 Tordoir, J., 2011. Clinical study protocol for the ARCH project - computational
202 modeling for improvement of outcome after vascular access creation. J Vasc Access 12,
203 369-376.

204 Caroli, A., Manini, S., Antiga, L., Passera, K., Ene-Iordache, B., Rota, S., Remuzzi, G., Bode,
205 A., Leermakers, J., van de Vosse, F.N., Vanholder, R., Malovrh, M., Tordoir, J.,
206 Remuzzi, A., 2013. Validation of a patient-specific hemodynamic computational model
207 for surgical planning of vascular access in hemodialysis patients. Kidney Int 84, 1237-
208 1245.

209 Chiu, J.J., Chien, S., 2011. Effects of disturbed flow on vascular endothelium:
210 pathophysiological basis and clinical perspectives. Physiol Rev 91, 327-387.

211 Davies, P.F., 2009. Hemodynamic shear stress and the endothelium in cardiovascular
212 pathophysiology. Nat Clin Pract Cardiovasc Med 6, 16-26.

213 De Santis, G., De Beule, M., Van Canneyt, K., Segers, P., Verdonck, P., Verhegghe, B.,
214 2011. Full-hexahedral structured meshing for image-based computational vascular
215 modeling. Med Eng Phys, 1318-1325.

216 De Santis, G., Mortier, P., De Beule, M., Segers, P., Verdonck, P., Verhegghe, B., 2010.
217 Patient-specific computational fluid dynamics: structured mesh generation from coronary
218 angiography. Med Biol Eng Comput 48, 371-380.

219 Ene-Iordache, B., Cattaneo, L., Dubini, G., Remuzzi, A., 2013. Effect of anastomosis angle
220 on the localization of disturbed flow in 'side-to-end' fistulae for haemodialysis access.
221 Nephrol Dial Transplant 28, 997-1005.

222 Ene-Iordache, B., Remuzzi, A., 2012. Disturbed flow in radial-cephalic arteriovenous fistulae
223 for haemodialysis: low and oscillating shear stress locates the sites of stenosis. Nephrol
224 Dial Transplant 27, 358-368.
225 He, X., Ku, D.N., 1996. Pulsatile flow in the human left coronary artery bifurcation : average
226 conditions. J. Biomech. Eng. 118, 74-82.
227 He, Y., Terry, C.M., Nguyen, C., Berceli, S.A., Shiu, Y.T., Cheung, A.K., 2013. Serial
228 analysis of lumen geometry and hemodynamics in human arteriovenous fistula for
229 hemodialysis using magnetic resonance imaging and computational fluid dynamics. J
230 Biomech 46, 165-169.
231 Himburg, H.A., Friedman, M.H., 2006. Correspondence of low mean shear and high
232 harmonic content in the porcine iliac arteries. J Biomech Eng 128, 852-856.
233 Jia, L., Wang, L., Wei, F., Yu, H., Dong, H., Wang, B., Lu, Z., Sun, G., Chen, H., Meng, J.,
234 Li, B., Zhang, R., Bi, X., Wang, Z., Pang, H., Jiang, A., 2015. Effects of wall shear stress
235 in venous neointimal hyperplasia of arteriovenous fistulae. Nephrology.
236 Lee, S.W., Smith, D.S., Loth, F., Fischer, P.F., Bassiouny, H.S., 2007. Importance of flow
237 division on transition to turbulence within an arteriovenous graft. J Biomech 40, 981-
238 992.
239 Leermakers, J.J., Bode, A.S., Vaidya, A., van der Sande, F.M., Evers, S.M., Tordoir, J.H.,
240 2013. Cost-effectiveness of vascular access for haemodialysis: arteriovenous fistulas
241 versus arteriovenous grafts. Eur J Vasc Endovasc Surg 45, 84-92.
242 Marie, Y., Guy, A., Tullett, K., Krishnan, H., Jones, R.G., Inston, N.G., 2014. Patterns of
243 blood flow as a predictor of maturation of arteriovenous fistula for haemodialysis. J Vasc
244 Access 15, 169-174.

McGah, P.M., Leotta, D.F., Beach, K.W., Aliseda, A., 2014. Effects of wall distensibility in hemodynamic simulations of an arteriovenous fistula. Biomech Model Mechanobiol 13, 679-695.

McGah, P.M., Leotta, D.F., Beach, K.W., Eugene Zierler, R., Aliseda, A., 2013. Incomplete restoration of homeostatic shear stress within arteriovenous fistulae. J Biomech Eng 135(1), 011005.

Niemann, A.K., Udesen, J., Thrysoe, S., Nygaard, J.V., Frund, E.T., Petersen, S.E., Hasenkam, J.M., 2010. Can sites prone to flow induced vascular complications in a-v fistulas be assessed using computational fluid dynamics? J Biomech 43, 2002-2009.

NKF/KDOQI, 2006. Clinical practice guidelines for vascular access.

Peiffer, V., Sherwin, S.J., Weinberg, P.D., 2013. Computation in the rabbit aorta of a new metric - the transverse wall shear stress - to quantify the multidirectional character of disturbed blood flow. J Biomech 46, 2651-2658.

Remuzzi, A., Ene-Iordache, B., 2013. Novel paradigms for dialysis vascular access: upstream hemodynamics and vascular remodeling in dialysis access stenosis. Clin J Am Soc Nephrol, 8(12), 2186-2193.

Sigovan, M., Rayz, V., Gasper, W., Alley, H.F., Owens, C.D., Saloner, D., 2013. Vascular remodeling in autogenous arterio-venous fistulas by MRI and CFD. Ann Biomed Eng 41, 657-668.

OpenFOAM team, 2014. The OpenFOAM Foundation. (http://www.openfoam.org).

Vassalotti, J.A., Jennings, W.C., Beathard, G.A., Neumann, M., Caponi, S., Fox, C.H., Spergel, L.M., Fistula First Breakthrough Initiative Community Education, 2012. Fistula first breakthrough initiative: targeting catheter last in fistula first. Semin Dial 25, 303-310.

Walsh, M.T., Kavanagh, E.G., O'Brien, T., Grace, P.A., McGloughlin, T., 2003. On the existence of an optimum end-to-side junctional geometry in peripheral bypass surgery--a computer generated study. Eur J Vasc Endovasc Surg 26, 649-656.

TABLES

Table 1. Geometric and haemodynamic features of the patient-specific AVF model.

	Diameter *(mm)*	Volumetric flow rate *(mL/min)*	Re	Wo
PA inlet	5	844 (1,121; 669)	1,387 (1,879; 1,080)	3.91 (3.95; 3.88)
DA inlet	3.8	86 (168; -60)	161 (338; 106)	2.76 (2.87; 2.69)
V outlet	5.9	930 (1,283; 639)	1,263 (1,788; 837)	4.52 (4.58; 4.44)

Note: Waveforms of the flow rate in the PA and DA are shown in Figure 1. The flow rate in V is obtained by their summation. Re and Wo numbers are calculated for the given diameters and expressed as time-averaged and (maximum; minimum) values over the pulse cycle.

Legend: PA, proximal (radial) artery; DA, distal (radial) artery; V, (cephalic) vein; Re, Reynolds number; Wo, Womersley number.

Table 2. Characteristics of near-wall flow at four feature points on the AVF surface.

Point	Position	Type of bulk flow	TKE	Type of disturbed flow	OSI	transWSS	max WSS	min WSS	TAWSS
			(cm^2/s^2)			*($dyne/cm^2$)*	*($dyne/cm^2$)*	*($dyne/cm^2$)*	*($dyne/cm^2$)*
P1	PA (inner wall)	laminar	89.2	-	0	0.7	110.2	59.0	78.9
P2	DA	laminar	37.1	reciprocating	0.42	1.2	9.4	-23.0	0.7
P3	SS (inner wall)	turbulent	270.1	reciprocating, multidirectional	0.47	22.7	92.4	-119.2	2.1
P4	V (outer wall)	turbulent (damped)	203.9	multidirectional	0.003	6.1	118.7	29.3	66.7

Note: The position of the four feature points are as shown in Figure 2a (right).

Legend: PA, proximal (radial) artery; DA, distal (radial) artery; SS, swing segment; V, vein (cephalic); OSI, oscillatory shear index; WSS, wall shear stress; transWSS, transverse WSS; TAWSS, time-averaged WSS; TKE, turbulent kinetic energy (see Supplemental data on-line).

LEGENDS TO FIGURES

Figure 1. a) Patient-specific blood volumetric flow rate waveforms derived from US pulsed-Doppler velocity spectra images. Continuous and dashed curves represent the blood flow in the PA and DA, respectively. Blood flow in the DA changes direction during the cardiac cycle, negative is antegrade (towards the hand) and positive is retrograde flow. Horizontal lines indicate the time-averaged blood flow rate over the cardiac cycle, 844 mL/min for PA and 86.5 mL/min for DA, respectively. b) 3-D surface of the model and detail of the surface and volume meshwork showing internal cells and the boundary layers near the wall. Legend: PA, proximal artery; DA, distal artery. Arrows indicate the main direction of blood flow.

Figure 2. Distribution of haemodynamic wall parameters on the AVF wall: a) plot of OSI; b) plot of tranWSS. Values of OSI between 0 and 0.1 and of transWSS below 10 dyne/cm^2 were represented in light grey to emphasize the pattern of disturbed flow on the AVF surface. Left, front view; right, rear view of the AVF.

Figure 3. Plot of WSS vector magnitude variation throughout the cardiac cycle for four feature points on the AVF surface. The sign of the WSS vector was taken into account by considering positive the direction of the bulk flow. Position of feature points (P1 to P4) on the AVF surface are as depicted in Figure 2a right. The characteristics of near-wall disturbed flow adjacent to these points are summarized in Table 2.

Continuous line, WSS magnitude; dashed line, time-averaged WSS over the pulse cycle.

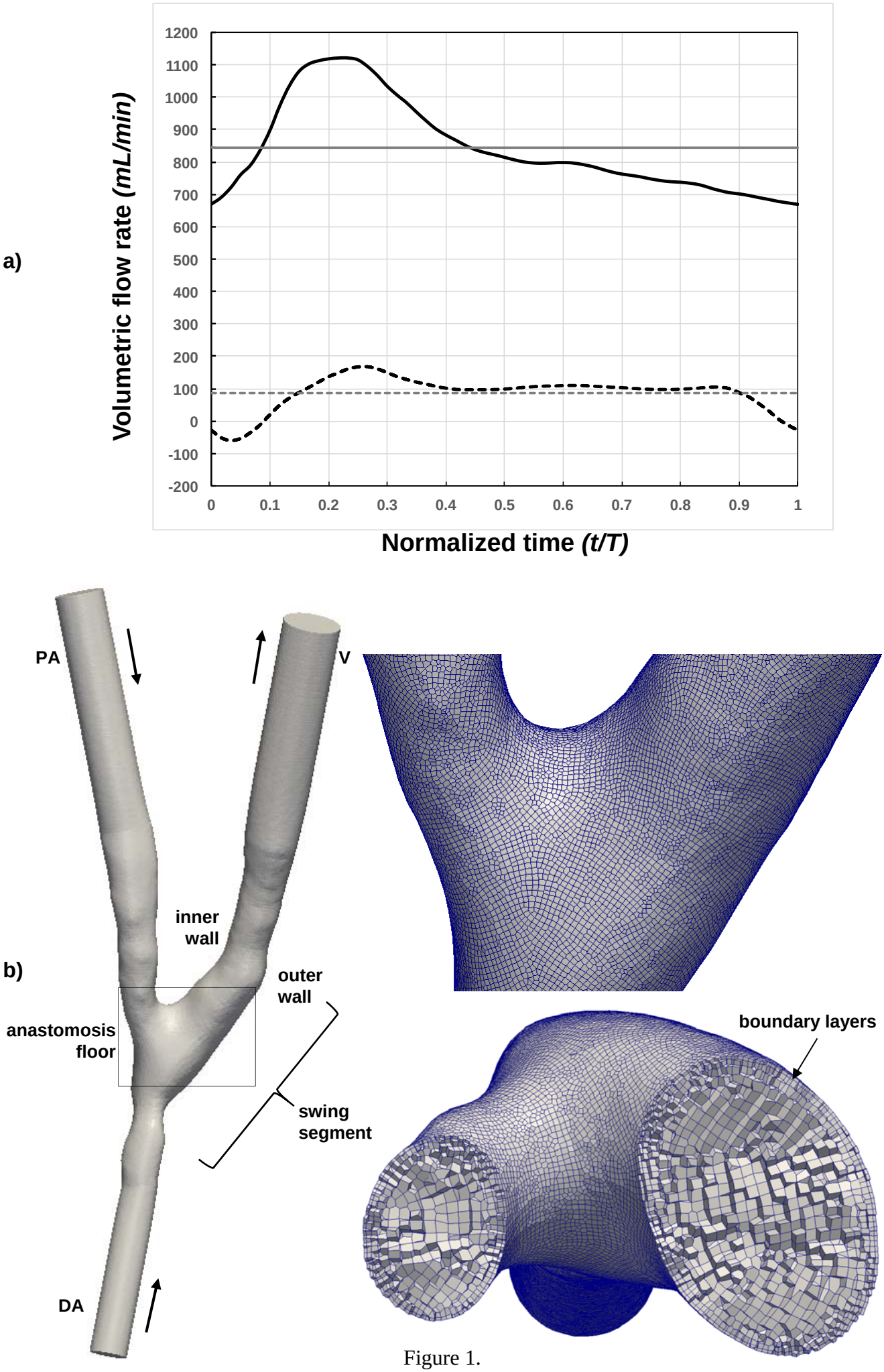
a)
Volumetric flow rate (mL/min)
1200
1100
1000
900
800
700
600
500
400
300
200
100
0
-100
-200
0
0.1
0.2
0.3
0.4
0.5
0.6
0.7
0.8
0.9
1
Normalized time (t/T)
b)
PA
V
inner wall
outer wall
anastomosis floor
swing segment
DA
boundary layers

Figure 1.

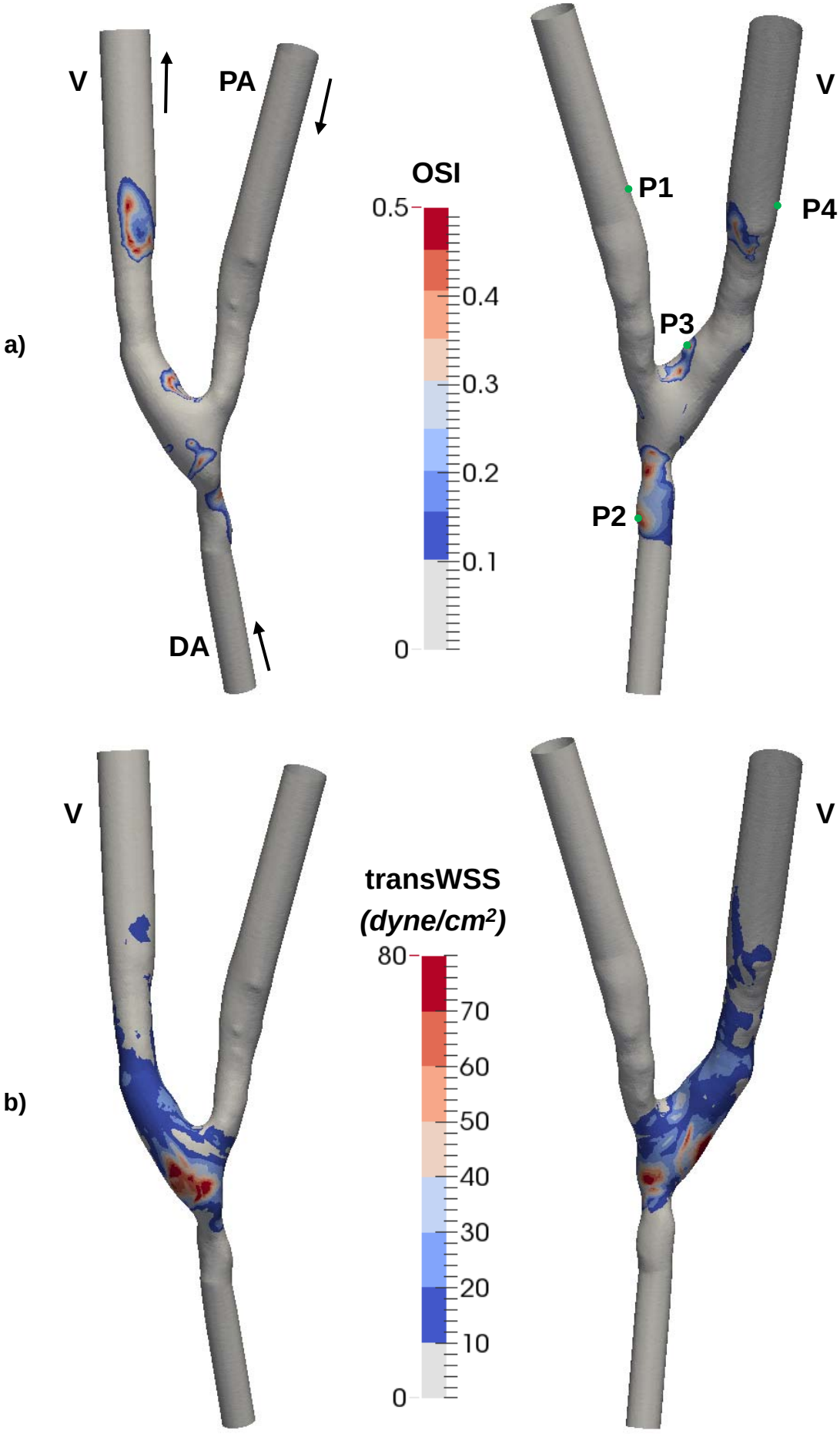
a)
V
PA
DA
OSI
0.5
0.4
0.3
0.2
0.1
0
V
P1
P4
P3
P2
b)
V
transWSS
(dyne/cm²)
80
70
60
50
40
30
20
10
0
V

Figure 2.

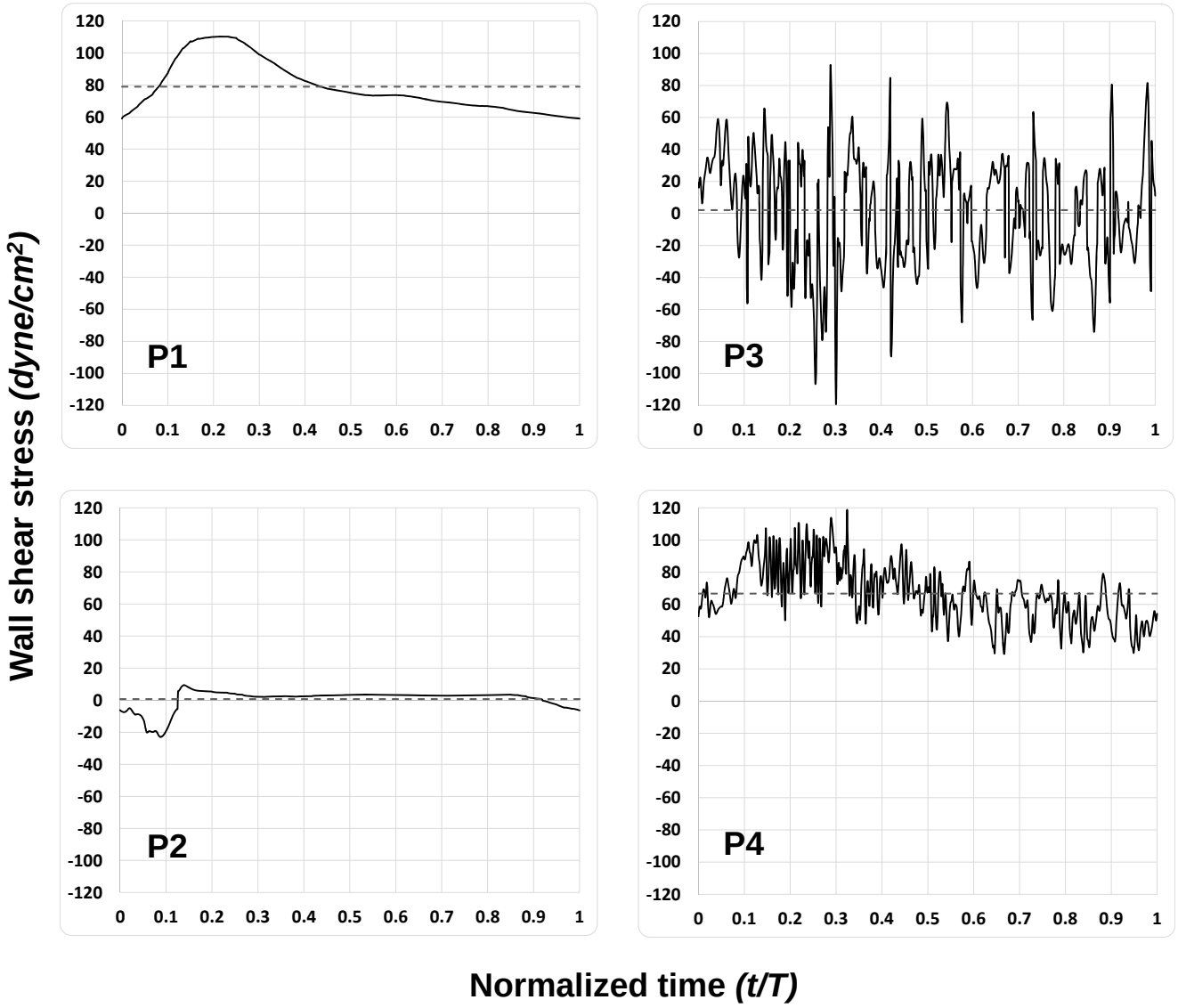
Wall shear stress (dyne/cm²)
P1
P2
P3
P4
120
100
80
60
40
20
0
-20
-40
-60
-80
-100
-120
0 0.1 0.2 0.3 0.4 0.5 0.6 0.7 0.8 0.9 1
Normalized time (t/T)

Figure 3.